Journal of Alloys and Compounds 725 (2017) 253–259

Contents lists available at ScienceDirect

Journal of Alloys and Compounds

journal homepage: http://www.elsevier.com/locate/jalcom

High-response NO_2 resistive gas sensor based on bilayer MoS_2 grown by a new two-step chemical vapor deposition method

Tingting Xu, Yongyong Pei, Yunyun Liu, Di Wu, Zhifeng Shi, Junmin Xu*, Yongtao Tian, Xinjian Li**

Department of Physics and Engineering, and Key Laboratory of Material Physics, Zhengzhou University, Zhengzhou 450052, PR China

ARTICLE INFO

Article history:
Received 14 March 2017
Received in revised form
7 June 2017
Accepted 9 June 2017
Available online 12 June 2017

Keywords:
Bilayer MoS_2
Resistive gas sensor
P-type
Sensitivity
Room temperature

ABSTRACT

MoS_2 atomic layers with a lateral grain size of 50–100 μm were synthesized by a new two-step chemical vapor deposition method. The product was confirmed to be bilayer MoS_2 by the characterization of Raman spectroscopy, atomic force microscopy and high-resolution transmission electron microscopy. The growth mechanism and the influencing factors during the growth process of the bilayer MoS_2 were proposed and the so-obtained large lateral grain sizes of MoS_2 atomic layers were attributed to the high surface mobility and enhanced surface evaporation. The resistive gas sensors based on as-prepared bilayer MoS_2 films showed a p-type character and achieved a superior sensitivity of 2.6% to 1 ppm NO_2 gas at room temperature.

1. Introduction

The increasing concern to daily life, environmental protection, industrial and agricultural production monitoring has given rise to a keen interest in gas detection [1,2]. Because of the emissions of fossil-fuel combustion and the exhaust fumes of cars, NO_2 is one of the most common air pollutants among various gases. NO_2 exposure can result in skin damage and respiratory disorders, and a 5 min emergency exposure limit for 35 ppm NO_2 has been proposed by the American Industrial Hygiene Association. Thus, a sensitive sensor is highly needed to monitor the NO_2 concentrations timely. In the past few decades, metal oxide semiconductors have been extensively studied as gas-sensing materials due to the low cost and easy preparation [3]. However, the high working temperature of gas sensors based on metal oxides [4] and the resulting safety problem have impeded their practical applications. To this respect, searching for suitable sensing materials has been an urgent task.

Because of the unique two dimensional microstructure, graphene and the similar two-dimensional materials have attracted world-wide interests [5–12]. Nevertheless, graphene's zero bandgap energy and the resulting high leakage current have limited many applications in electronics [13]. MoS_2 is a graphene-like layered semiconductor with a bandgap in the range of 1.2–1.9 eV, and its bandgap is dependent on the thickness [14,15]. When the thickness of MoS_2 decreases to monolayer, the pristine indirect bandgap transfers into a direct one. Due to the semiconducting property, it's possible for MoS_2 to form p-n junctions with other semiconducting materials [16,17]. The obtained p-n junction is a new type of sensing device and will enhance the sensing properties significantly. It was reported that the sensitivity of the MoS_2-TiO_2 heterojunction to alcohol increased almost 11 times than that of TiO_2 nanotubes [18]. What's more, due to the large surface-to-volume ratios and inherent flexibility of few-layered MoS_2, gas sensors based on few-layered MoS_2 are attracting more and more attentions. So far, MoS_2 has exhibited a significant response to various gases (such as NO_2, NO, NH_3, H_2) at room temperature [16,19–21], and has been considered as a promising gas-sensing material.

Field Effect Transistors (FET) [22] and resistive gas sensors [23–25] based on few-layered MoS_2 or MoS_2 flakes have been used for gas sensing. As the fabrication of FET is quite elaborate, resistive gas sensors based on layered MoS_2 with standard interdigitated electrodes are more suitable for practical application. However, for the fabrication of resistive gas sensors based on layered MoS_2, the

* Corresponding author.
** Corresponding author.
E-mail addresses: xutt@zzu.edu.cn (T. Xu), JunminXu@zzu.edu.cn (J. Xu), lixj@zzu.edu.cn (X. Li).

http://dx.doi.org/10.1016/j.jallcom.2017.06.105
0925-8388/

large-scale synthesis of high-quality and uniform MoS_2 atomic layers using an easy and low-cost method is still a challenge. Mechanical Exfoliation is a typical top-down approach to obtain MoS_2 atomic layers and has received considerable attention [26,27]. Nevertheless, the non-uniform thickness and small size undermine the viability of such approaches. Similar limitations exist with other top-down methods, e.g. laser thinning [28] and liquid exfoliation [29], as well as the hydrothermal reaction method [30]. More recently, atomic layer deposition (ALD) have also been introduced to synthesize large-area ultra-thin MoS_2 films [31,32], but the complicated process and expensive cost restricted its development. Chemical vapor deposition (CVD), a typical bottom-up method, is a scalable uniform and high-quality MoS_2 synthesis technique. Large-area MoS_2 atomic layers have been synthesized by direct sulfuration of pre-deposited molybdenum thin films by magnetron sputtering technique [33,34]. The size and thickness of the film can roughly be tuned by controlling the size of the substrate and the thickness of molybdenum film. However, the small lateral grain size induced the reduction of the quality of as-synthesized MoS_2. Although high-quality and large-area MoS_2 atomic layers were obtained by the sulfuration of ammonium tetrathiomolybdate films [35], the complexity in precursor preparation and expensive precursor limited its feasibility. Due to the low melting and evaporation temperatures, Molybdenum trioxide (MoO_3) and sulfur powders have been widely used as the precursors to synthesize MoS_2 by a CVD method. Traditionally, the evaporation and sulfuration of MoO_3 powder are carried out at the same time in a tube furnace, and the lateral-to-vertical ratio of growth rates is dominated by temperatures, pressures, gas flows, etc [36,37]. So far, it's still a challenge in controlling the lateral-to-vertical ratio of growth rates and thus the resultant lateral grain sizes with atomic thickness.

Herein, a new method, in which the deposition and sulfuration of MoO_3 were carried out in two separate steps, was adopted to synthesize MoS_2 atomic layer with a large lateral grain size. The resistive gas sensors based on as-prepared bilayer MoS_2 films showed a p-type character and manifested a good sensitivity and selectivity to NO_2 gas at room temperature.

2. Experimental

2.1. Synthesis and characterization of MoS_2

Here a new approach of growing ultrathin MoS_2 films was presented. The MoS_2 films were prepared on SiO_2/Si substrates in a tube furnace with multiple temperature zones by a CVD method, and the growth process can be divided into two steps: deposition of MoO_3 and sulfuration of MoO_3 (as shown in Fig. 1c). Fig. 1a and b schematically illustrate our experimental set-up and temperature-time curve during the sulfuration of MoO_3. In the first step, High purity MoO_3 powder (99.9%, 10 mg) was placed in an alumina boat at the center of the second temperature zone and the SiO_2/Si substrates were placed at the down stream of the MoO_3 powder. After the temperature of the MoO_3 powder was kept at 750 °C for 5min, the MoO_3 powder was thermally evaporated and MoO_3 films were obtained on SiO_2/Si substrates. In the second step, the MoO_3 films were placed at the down stream of sulfur powder (99.99%, >1 g) and were reduced by sulfur vapor in gas phase at 650 °C under atmospheric pressure (as shown in Fig. 1a). Finally, ultrathin MoS_2 films formed on SiO_2/Si substrates after the full sulfuration of MoO_3 films. It is worth mentioning that the SiO_2/Si substrates used in the growth process were cleaned or treated in advance with acetone, alcohol, deionized water, and O_2 plasma for 180s successively.

The as-prepared MoS_2 films were characterized by X-ray diffraction with Cu Kα radiation (XRD PA National X′ Pert Pro), X-ray photoelectron spectroscopy (XPS, AXIS Supra), Raman spectroscopy (HORIBA, LabRAM HR Evolution), atomic force microscopy (AFM, NT-MDT, Prima) and high-resolution transmission electron microscopy (HRTEM, JEOL, JEM-2100).

2.2. Fabrication and testing of the resistive gas sensors based on as-prepared MoS_2 films

After interdigital gold electrodes were fabricated on top of as-prepared MoS_2 films on the SiO_2/Si substrates by e-beam evaporation process, resistive gas sensors based on as-prepared MoS_2 films were obtained. The gas sensing properties of the as-fabricated gas sensors were measured by the CGS-1TP gas sensing measurement system (Beijing Elite Tech Co., Ltd, China). All the gas sensing measurements were carried out in an atmospheric environment and a relative humidity of 24%.

3. Results and discussion

3.1. Characterization of as-grown MoS_2 film

The optical image of as-grown MoS_2 (Fig. 2a) shows that the continuous MoS_2 film is formed by triangle flakes with a lateral grain size of 50–100 μm. All of the XRD diffraction peaks in the XRD patterns (Fig. 2b) are ascribed to hexagonal MoS_2 (JCPDS-ICDD 06-0097), and no diffraction peaks of the impurity phase are observed, indicating a single phase MoS_2 was obtained. The prominent diffraction peak is attributed to the (002) crystal plane. XPS was used to determine the chemical composition of the as-grown MoS_2 films, and the results are demonstrated in Fig. 2c and d. The Mo 3d spectrum exhibits a clear doublet along with a small S 2s peak, and the peaks present at 232.3 eV, 229.2 eV and 226.5 eV correspond to the Mo $3d_{3/2}$, Mo $3d_{5/2}$ and S 2s orbit, respectively. Similarly, the S 2p spectrum shows a doublet, with the $2p_{1/2}$ peak at 163.2 eV and the $2p_{3/2}$ peak at 161.9 eV. The observed binding energies in this work are consistent with the values for MoS_2 reported in previous work [38]. What's more, the S: Mo ratio measured from the XPS spectra is close to 2, confirming the stoichiometry of MoS_2.

Raman and AFM were used to evaluate the thickness and quality of the as-grown MoS_2 films. Herein, Raman spectra of the bulk MoS_2 and as-grown MoS_2 films were measured by using a 432 nm laser with a power below 1 mW at room temperature. E^1_{2g} and A_{1g} are two characteristic Raman peaks for MoS_2, which represent the in-plane and out-of-plane vibration of Mo-S bond, respectively. Here the peak frequency difference between E^1_{2g} and A_{1g} is defined as Δ. For bulk MoS_2, the value of Δ is 25 cm^{-1}. The value of Δ is found to decrease with the decrease of the number of MoS_2 layers, and can be used to determine the number of MoS_2 layers [39]. Compared to bulk MoS_2, the E^1_{2g} peak is observed to increase, whereas the A_{1g} peak is observed to decrease in frequency (as shown in Fig. 3a). The E^1_{2g} and A_{1g} peak of as-grown MoS_2 film are located at 385.8 $cm^{-1}cm^{-1}$ and 407.2 cm^{-1}, respectively, and the value of Δ is 21.4 cm^{-1}, indicating that bilayer MoS_2 was obtained. What's more, the AFM characterization confirmed that the thickness of the synthesized bilayer MoS_2 is 1.39 nm (Fig. 3b and c), and the thickness is in consistence with that reported in the previous work [39].

After as-grown MoS_2 films on the SiO_2/Si substrate were transferred on a copper grid [36], TEM was also performed to further investigate the structures of the as-grown MoS_2 bilayer films on the atomic scale. The edge of the MoS_2 films can be clearly seen in Fig. 3d, demonstrating the as-grown sample is bilayer MoS_2. What's more, the distance between the adjacent layers is about 6.5 Å (shown in Fig. 3d) [33]. The high resolution TEM image and the corresponding selected area electron diffraction (SAED) pattern

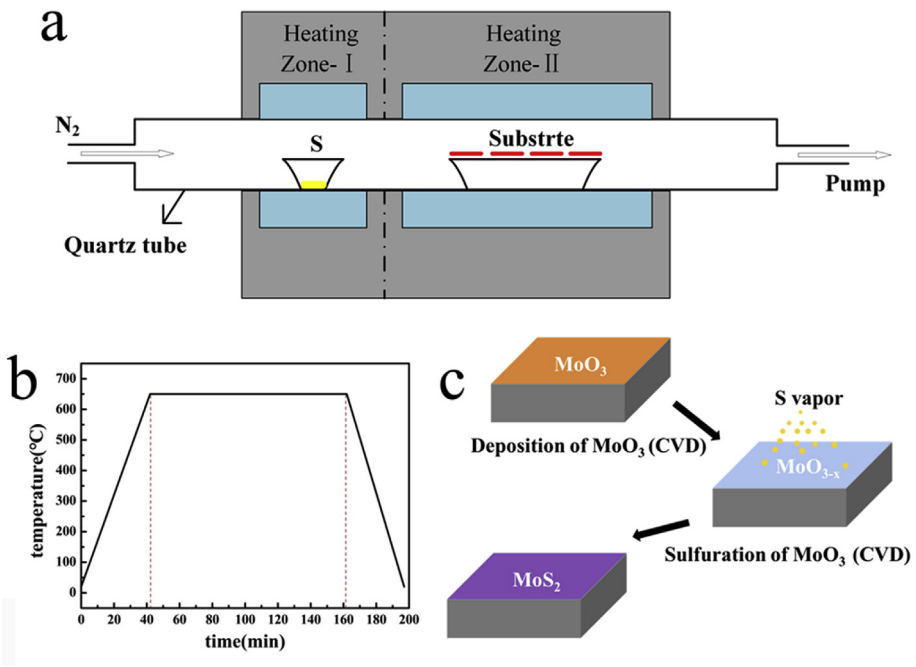

Fig. 1. (a) Schematic illustration of the MoS_2 synthesis setup by CVD; (b) temperature-time curve during the sulfuration of MoO_3; (c) Schematic illustration of the growth process of the MoS_2 film.

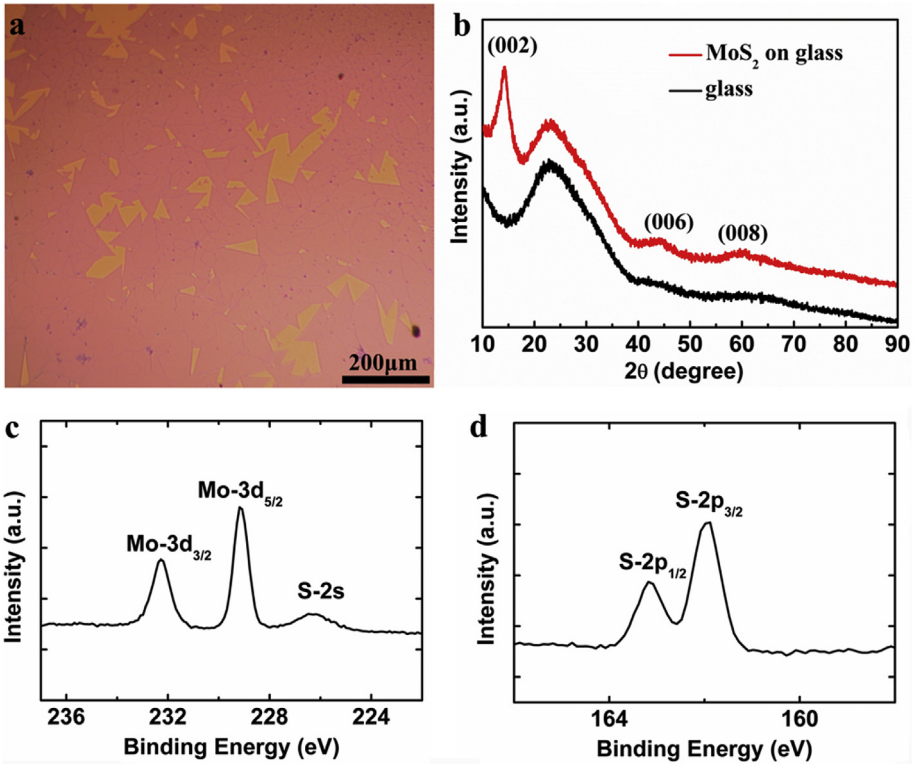

Fig. 2. Optical image (a) and XRD pattern (b) of as-prepared MoS_2 film; (c) and (d) Core binding energies determined by XPS spectra, Mo 3d peaks are present at 232.3 eV and 229.2 eV, with S 2s at 226.5 eV, S peaks are present at 163.2 eV and 161.9 eV.

of as-grown MoS_2 film are shown in Fig. 3e and f. The lattice spacings of 2.7 and 1.6 Å in Fig. 3e correspond to the (100) and (110) planes of hexagonal MoS_2, respectively, and these two planes belong to the [001] zone axis. The diffraction spots of MoS_2 (110) and (100) planes are shown in the SAED pattern in Fig. 3f.

3.2. Growth mechanics of MoS_2 atomic layer

After the deposition of MoO_3 by a CVD method, a MoO_3 film was obtained on the SiO_2/Si substrates. During the sulfuration process of the MoO_3 film, the reaction mechanism is shown in the reaction

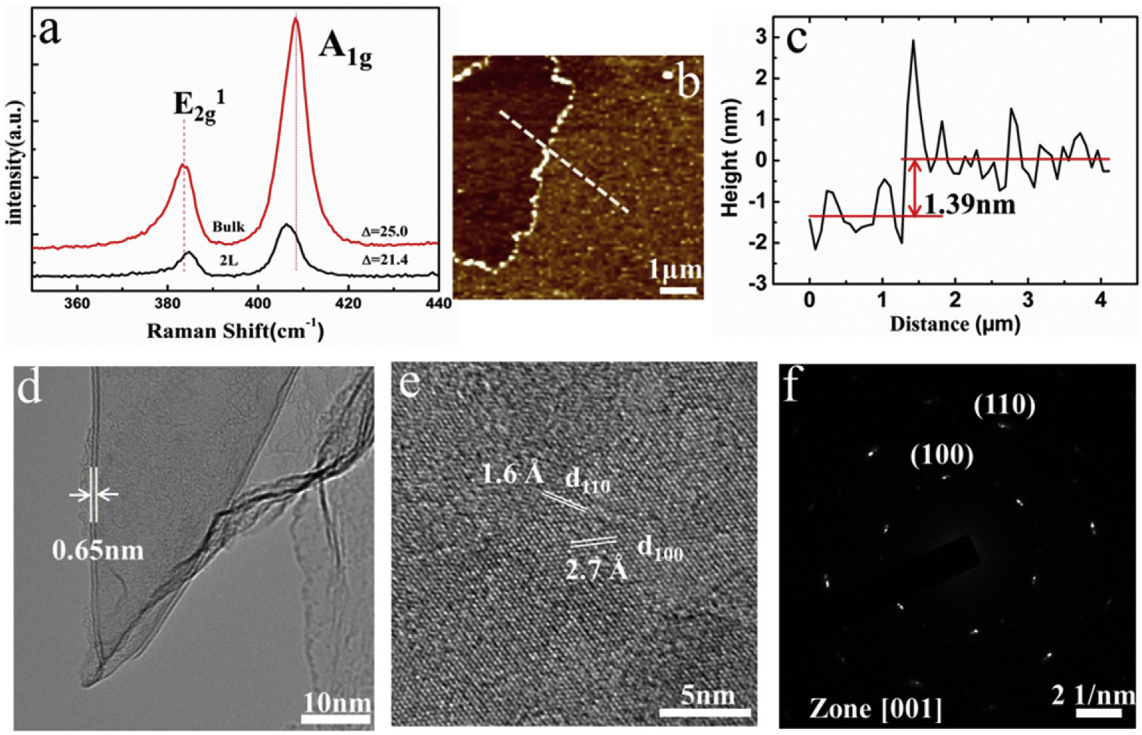

Fig. 3. (a) The Raman spectrum with two active modes (E_{2g}^1 and A_{1g}) of as-grown MoS_2; (b) AFM image of as-grown MoS_2; (c) AFM height profiles along the white dash line in (b); (d) TEM image of the edge of as-grown MoS_2 film; (e) The high resolution TEM image of as-grown MoS_2 film, and the lattice spacing of 2.7 Å and 1.6 Å corresponding to the (100) and (110) plane of hexagonal MoS_2; (f) The SAED pattern of the MoS_2 film in (e).

equations (1) and (2).

$$MoO_3 + S = MoS_{3-x} + SO_2 \quad (1)$$

$$MoS_{3-x} + S = MoS_2 + SO_2 \quad (2)$$

First of all, the surface of MoO_3 film was reduced by sulfur vapor, and an intermediate product MoO_{3-x} was formed. Afterwards, in the continuous sulfur vapor, MoS_2 was obtained after the reduction of MoO_{3-x}. The thickness and lateral grain size of the as-prepared MoS_2 are determined by the thickness of the as-deposited MoO_3 film by the CVD method, as well as the following sulfuration temperature [34]. The thickness of the MoO_3 film was affected by the weight of the MoO_3 powder, the growing temperature, the gas flow, etc. MoS_2 atomic layers with a lateral grain size of 50–100 μm were obtained in this work, while the lateral grain sizes of obtained MoS_2 synthesized by sulfurating the sputtered Mo thin films are only 100 nm [33,34]. The larger lateral grain size in this work can be attributed to the much weaker adhesion between the as-deposited MoO_3 film by a CVD method and the substrate, since a weak adhesion can result in high surface mobility and enhanced surface evaporation.

3.3. Gas sensing properties of the resistive gas sensors based on as-prepared MoS_2 films

The schematic diagram for the resistive gas sensor based on as-synthesized MoS_2 films is shown in Fig. 4a. The sensitivity of as-fabricated gas sensors was defined as $\Delta R/R_a=(R_g-R_a)/R_a$, where R_a and R_g are the measuring resistances of the gas sensors in ambient air and the target gas, respectively. Response and recovery time are defined as the time it takes the sensor to reach 90% of the saturation value in a NO_2 atmosphere and 10% of the base value in air, respectively. The typical transient response-recovery curve of as-fabricated gas sensors to NO_2 of different concentrations at room temperature is shown in Fig. 4b. It is shown that the resistance of the sensor decreased rapidly after the injection of NO_2 gas, and it can recover to the initial value after the NO_2 gas was released. No baseline shift in the response-recovery curve was discovered in the whole testing process. The responses of as-fabricated gas sensors as a function of NO_2 concentration are shown in Fig. 4c. The sensitivity increased with the increasing concentration of NO_2 from 1 to 100 ppm, which is approximately 2.6%, 3.9%, 8.4%, 10.8%, 12.6%, 17.1%, 26.4% for 1, 2, 5, 10, 20, 50, 100 ppm NO_2 gas, respectively. When the as-fabricated gas sensor was exposed to 1 ppm NO_2, the sensing signal experienced low noise. Therefore, 1 ppm can be defined as the lower detection limit of the sensor to NO_2 gas based on a signal (S)-to-noise (N) ratio (S/N > 3). For 1 ppm NO_2, the response and recovery times of the gas sensor are 11.3 min and 5.3 min, respectively. The sensitivities of the gas sensor to O_2, H_2, CH_4 and NH_3 with the same concentration of 50 ppm at room temperature were also measured. The gas sensor showed weaker responses to the other gases than to NO_2, indicating a good NO_2 selectivity against O_2, H_2, CH_4 and NH_3.

It is important to note that the resistance of the as-prepared MoS_2 films decreased upon exposure to oxidative gases (NO_2, O_2) and increased upon exposure to reductive gases (H_2, CH_4 and NH_3). A widely accepted model of the gas sensing mechanism suggests that upon exposure to reductive gas, chemisorbed oxygen on the semiconductor surface will react with the reductive gas species and the electrons trapped by oxygen will be released into the semiconductor, leading to a change in resistance. For *n*-type semiconductor, the resistance decreases due to the increase of electron concentration in the semiconductor. While for *p*-type semiconductor, the resistance increases because of the combination of holes with electrons released from surface reaction. Upon exposure

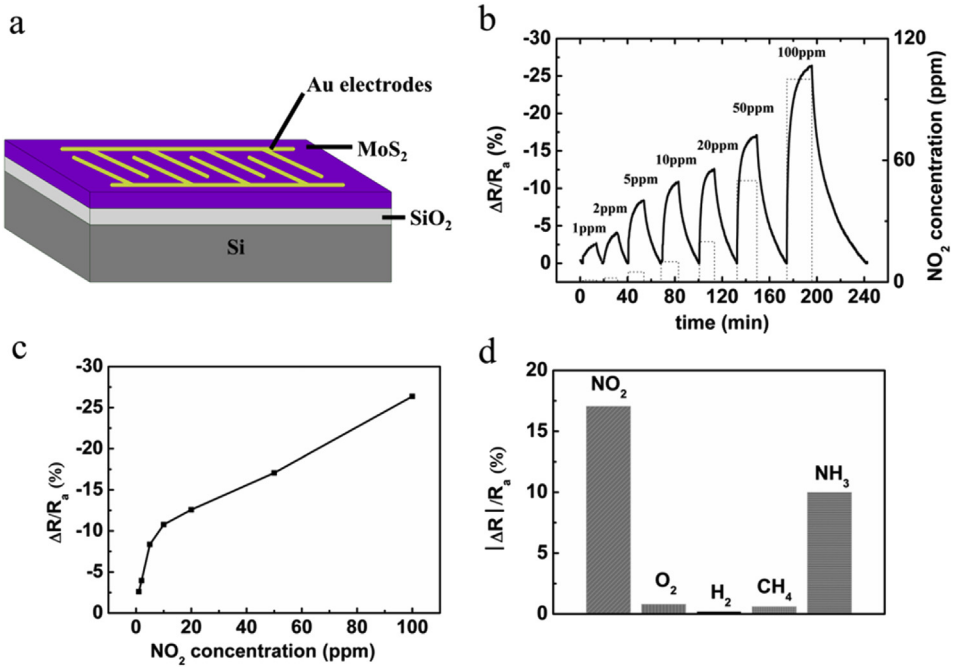

Fig. 4. (a) The schematic diagram for the resistive gas sensor based on as-synthesized MoS_2 films; (b) The transient response-recovery curve of as-fabricated gas sensors to NO_2 of different concentrations at room temperature. (c) Responses of as-fabricated gas sensors as a function of NO_2 concentration. (d) Responses of as-fabricated gas sensors to 50 ppm NO_2, O_2, H_2, CH_4, NH_3 at room temperature.

to oxidative gases, the gas species act as acceptors, leading to resistance increase for *n*-type semiconductor and decrease for *p*-type semiconductor. In view of the changing resistance upon exposed to oxidative and reductive gases, it can be concluded that the as-prepared MoS_2 films showed typical characteristics of a *p*-type semiconductor. What's more, the similar *p*-type characteristics of MoS_2 have been also reported in previous work [24], and the obtained p-type MoS_2 films can be attributed to the N substitutional doping of S vacancies in the growth process [24].

The sensing mechanism of the as-synthesized p-type MoS_2 can be described as follows. When the p-type MoS_2 was initially exposed to the air, oxygen molecules was chemisorbed on the surface, took away some electrons form the valence band and oxygen species (O_2^-, O^-) was formed, leading to an increase in hole concentration and a decrease in resistance. When the p-type MoS_2 was then exposed to the oxidizing NO_2 gas, NO_2 molecules was chemisorbed as NO_2^- ions, which further extracted electrons from the valence band and increased the hole concentration. A hole-accumulation layer was created at the surface of MoS_2 by chemisorption of NO_2. The generation of holes made the p-type MoS_2 more conductive. When the supply of NO_2 is stopped and the p-type MoS_2 was exposed to air again, the adsorbed NO_2^- species evaporated, leaving behind the captured electrons in the p-type MoS_2. The following electron-hole compensation process resulted in a decreasing hole concentration and an increase in resistance. At the end of the electron-hole compensation process, the resistance of the p-type MoS_2 returned to the original value. Inversely, when the p-type MoS_2 was exposed to the reducing H_2, CH_4 or NH_3, electrons extracted by the chemisorbed oxygen species (O_2^-, O^-) were released back to the valence band of the p-type MoS_2 and combined with the holes in the valence band, resulting in the increase of the resistance.

The reported lower detection limits, the corresponding sensitivities and the response/recovery time to NO_2 gas of resistive gas sensors based on MoS_2 nanostructures and other similar sensing materials were listed in Table 1, and most of them were tested at room temperature. Among the resistive gas sensors, the one based on MoS_2 nanosheets decorated with SnO_2 nanocrystals possesses the minimum lower detection limit of 0.5 ppm and the shortest response/recovery time, and the corresponding sensitivity is 0.6%. The sensitivity of the MoS_2/graphene heterostructure reached 3% to 1.2 ppm NO_2 gas, but this gas sensor device required a much higher working temperature of 150 °C. The as-synthesized bilayer MoS_2 film in the present work achieved a sensitivity of 2.6% to 1 ppm NO_2 gas at room temperature. The recovery time of as-synthesized bilayer MoS_2 film is much shorter than other similar sensing material (graphene oxide, graphene, ZnO-reduced graphene oxide nanocomposites) listed in Table 1, and ranks only second to MoS_2 nanosheets decorated with SnO_2 nanocrystals. Based on this, it can be concluded that this sensing property is outstanding among MoS_2 nanostructures and other similar sensing materials. As most of the MoS_2 nanostructures reported in the previous work in Table 1 were obtained by mechanical or chemical exfoliation methods, and as-synthesized MoS_2 nanostructures have the non-uniform thickness and small size. In the present work, MoS_2 atomic layer with uniform thickness was achieved in a tube furnace by a new two-step CVD method, and our production technique offers much better scope for scalability. What's more, the sensing properties demonstrated in the present work were tested in an atmospheric environment rather than a test environment, making it more attractive for practical application.

4. Conclusions

MoS_2 atomic layer was synthesized in a tube furnace by a new two-step CVD method, in which the deposition and sulfuration of MoO_3 were carried out successively. The Raman, AFM, TEM characterization displayed that the as-prepared MoS_2 is bilayer. The so-obtained bilayer MoS_2 with larger lateral grain sizes was attributed to the high surface mobility and enhanced surface evaporation. The

Table 1
Comparison of the sensitivity and the response/recovery time to NO_2 gas of resistive gas sensors based on different MoS_2 nanostructures and other similar sensing materials.

Nanostructures (synthesis method)	T (°C)	NO_2 (ppm)	Sensitivity (%)	T_{res} (min)	T_{rec} (min)	Reference
Bilayer MoS_2 film (CVD)	RT	1	2.6	11.3	5.3	Present work
MoS_2 nanoflakes (mechanical exfoliation)	27	5	n.q.	1	n.q.	[23]
MoS_2 flakes (chemical exfoliation)	RT	1	0	n.q.	n.q.	[24]
MoS_2 nanosheets decorated with SnO_2 nanocrystals (chemical exfoliation)	RT	0.5	0.6	1.3	1.4	[40]
MoS_2 film (sulfurizing a MoO_3 film)	RT	1.5	1	n.q.	n.q.	[25]
MoS_2/graphene heterostructure (mechanical exfoliation + CVD)	150	1.2	3	>5.6	11.2	[23]
Graphene oxide	25	5	40	40	43	[41]
Graphene (CVD)	22	1.5	3.2	>5	>20	[42]
ZnO-reduced graphene oxide nanocomposites	25	15	7.8	2.1	n.q.	[43]

Note: n.q. = not quantifiable since no equilibrium conditions were achieved. RT = room temperature. T_{res} = response time, T_{rec} = recovery time.

resistive gas sensors based on as-prepared bilayer MoS_2 films showed a p-type character and achieved a superior sensitivity of 2.6% to 1 ppm NO_2 gas at room temperature. This sensing property of the resistive gas sensor based on as-prepared MoS_2 films by the two-step CVD method represents an advance in the development of large-scale MoS_2 synthesis and gas sensor fabrication.

Acknowledgments

This work was supported by the National Natural Science Foundation of China (11504331), the China Postdoctoral Science Foundation (2015M582196, 2015M582193, 2015M582194), Educational Department of Henan Province (15A430048), the Outstanding Young Talent Research Fund of Zhengzhou University (1521317005, 1521317001), and the Startup Research Fund of Zhengzhou University (1411317010).

References

[1] C. Li, D. Yan, M. Wei, Layer-by-layer assembly of ordered organic–inorganic luminescent film toward sensoring nitrobenzene compound, Sens. Actuat. B 216 (2015) 198–203.
[2] H. Ma, R. Gao, D. Yan, J. Zhao, M. Wei, Organic–inorganic hybrid fluorescent ultrathin films and their sensor application for nitroaromatic explosives, J. Mater. Chem. C 1 (2013) 4128–4137.
[3] F. Gao, Y. Li, Y. Zhao, W. Wan, G. Du, X. Ren, H. Zhao, Facile synthesis of flower-like hierarchical architecture of SnO_2 nanoarrays, J. Alloys Compd. 703 (2017) 354–360.
[4] S. Ma, J. Jia, Y. Tian, L. Cao, S. Shi, X. Li, X. Chang, Improved H_2S sensing properties of Ag/TiO_2 nanofibers, Ceram. Int. 42 (2016) 2041–2044.
[5] K.S. Novoselov, A.K. Geim, S.V. Morozov, D. Jiang, M.I. Katsnelson, I.V. Grigorieva, S.V. Dubonos, A.A. Firsov, Two-dimensional gas of massless Dirac fermions in graphene, Nature 438 (2005) 197–200.
[6] B. Wang, Y. Wang, J. Park, H. Ahn, G. Wang, In situ synthesis of Co_3O_4/graphene nanocomposite material for lithium-ion batteries and supercapacitors with high capacity and supercapacitance, J. Alloys Compd. 509 (2011) 7778–7783.
[7] D.J. Late, B. Liu, J. Luo, A. Yan, H.S.S.R. Matte, M. Grayson, C.N.R. Rao, V.P. Dravid, GaS and GaSe ultrathin layer Transistors, Adv. Mater. 24 (2012) 3549–3554.
[8] R.V. Kashid, D.J. Late, S.S. Chou, Y.K. Huang, M. De, D.S. Joag, M.A. More, V.P. Dravid, Enhanced field-emission behavior of layered MoS_2 sheets, Small 9 (2013) 2730–2734.
[9] M. Thripuranthaka, R.V. Kashid, C. Sekhar Rout, D.J. Late, Temperature dependent Raman spectroscopy of chemically derived few layer MoS_2 and WS_2 nanosheets, Appl. Phys. Lett. 104 (2014) (081911-1-5).
[10] A.S. Pawbake, M.S. Pawar, S.R. Jadkar, D.J. Late, Large area chemical vapor deposition of monolayer transition metal dichalcogenides and their temperature dependent Raman spectroscopy studies, Nanoscale 8 (2016) 3008–3018.
[11] D.J. Late, Liquid exfoliation of black phosphorus nanosheets and its application as humidity sensor, Microporous Mesoporous Mater. 225 (2016) 494–503.
[12] Z. Jia, J. Xiang, F. Wen, R. Yang, C. Hao, Z. Liu, Enhanced photoresponse of SnSe-nanocrystals-decorated WS_2 monolayer phototransistor, ACS Appl. Mater. Interfaces 8 (2016) 4781–4788.
[13] M. Osada, T. Sasaki, 2D inorganic nanosheets: two-dimensional dielectric nanosheets: novel nanoelectronics from nanocrystal building blocks, Adv. Mater. 24 (2012) 209–228.
[14] B. Liu, W. Zhao, Z. Ding, I. Verzhbitskiy, L. Li, J. Lu, J. Chen, G. Eda, K.P. Loh, Engineering bandgaps of monolayer MoS_2 and WS_2 on fluoropolymer substrates by electrostatically tuned many-body effects, Adv. Mater. 28 (2016) 6457–6464.
[15] P. Liu, H. Li, L. Yang, B. Zhao, M. Li, B. Xiang, Rational synthesis of bandgap-tunable $MS_{2(1-x)}Se_{2x}$ (M=Mo, W) alloys and their physical properties, J. Alloys Compd. 710 (2017) 628–634.
[16] L. Hao, Y. Liu, W. Gao, Y. Liu, Z. Han, L. Yu, Q. Xue, J. Zhu, High hydrogen sensitivity of vertically standing layered MoS_2/Si heterojunctions, J. Alloys Compd. 682 (2016) 29–34.
[17] Y. Liu, L. Hao, W. Gao, Q. Xue, W. Guo, Z. Wu, Y. Lin, H. Zeng, J. Zhu, W. Zhang, Electrical characterization and ammonia sensing properties of MoS_2/Si p–n junction, J. Alloys Compd. 631 (2015) 105–110.
[18] P. Zhao, Y. Tang, J. Mao, Y. Chen, H. Song, J. Wang, Y. Song, Y. Liang, X. Zhang, One-Dimensional MoS_2-Decorated TiO_2 nanotube gas sensors for efficient alcohol sensing, J. Alloys Compd. 674 (2016) 252–258.
[19] P.K. Kannan, D.J. Late, H. Morgan, C.S. Rout, Recent developments in 2D layered inorganic nanomaterials for sensing, Nanoscale 7 (2015) 13293–13312.
[20] D.J. Late, Y.K. Huang, B. Liu, J. Acharya, S.N. Shirodkar, J. Luo, A. Yan, D. Charles, U.V. Waghmare, V.P. Dravid, C.N.R. Rao, Sensing behavior of atomically thin-layered MoS_2 transistors, ACS Nano 7 (2013) 4879–4891.
[21] Y. Niu, W. Jiao, R. Wang, G. Ding, Y. Huang, Hybrid nanostructures combining graphene–MoS_2 quantum dots for gas sensing, J. Mater. Chem. A 4 (2016) 8198–8203.
[22] B.L. Liu, L. Chen, G. Liu, A.N. Abbas, M. Fathi, C.W. Zhou, High-performance chemical sensing using schottky-contacted chemical vapor deposition grown monolayer MoS_2 Transistors, ACS Nano 8 (2014) 5304–5314.
[23] B. Cho, J. Yoon, S.K. Lim, A.R. Kim, D.H. Kim, S.G. Park, J.D. Kwon, Y.J. Lee, K.H. Lee, B.H. Lee, H.V. Ko, M.G. Hahm, Chemical sensing of 2D graphene/MoS_2 heterostructure device, ACS Appl. Mater. Interfaces 7 (2015) 16775–16780.
[24] M. Donarelli, S. Prezioso, F. Perrozzi, F. Bisti, M. Nardone, L. Giancaterini, C. Cantalini, L. Ottaviano, Response to NO_2 and other gases of resistive chemically exfoliated MoS_2-based gas sensors, Sens. Actuat. B 207 (2015) 602–613.
[25] B. Cho, M.G. Hahm, M. Choi, J. Yoon, A.R. Kim, Y.J. Lee, S.G. Park, J.D. Kwon, C.S. Kim, M. Song, Y. Jeong, K.S. Nam, S. Lee, T.J. Yoo, C.G. Kang, B.H. Lee, H.C. Ko, P.M. Ajayan, D.H. Kim, Charge-transfer-based gas sensing using atomic-layer MoS_2, Sci. Rep. 5 (2015) (8052-1-6).
[26] O. Lopez-Sanchez, D. Lembke, M. Kayci, A. Radenovic, A. Kis, Ultrasensitive photodetectors based on monolayer MoS_2, Nat. Nanotechnol. 8 (2013) 497–501.
[27] J. Wang, M. Yan, K. Zhao, X. Liao, P. Wang, X. Pan, W. Yang, L. Mai, Field Effect enhanced hydrogen evolution reaction of MoS_2 nanosheets, Adv. Mater. 29 (2017) (1604464-1-6).
[28] A. Castellanos-Gomez, M. Barkelid, A.M. Goossens, V.E. Calado, H.S.J. van der Zant, G.A. Steele, Laser-thinning of MoS_2: on demand generation of a single-layer semiconductor, Nano Lett. 12 (2012) 3187–3192.
[29] A. Jawaid, D. Nepal, K. Park, M. Jespersen, A. Qualley, P. Mirau, L.F. Drummy, R.A. Vaia, Mechanism for liquid phase exfoliation of MoS_2, Chem. Mater. 28 (2016) 337–348.
[30] X. Zhang, C. Shao, X. Li, F. Miao, K. Wang, N. Lu, Y. Liu, 3D MoS_2 nanosheet/TiO_2 nanofiber heterostructures with enhanced photocatalytic activity under UV irradiation, J. Alloys Compd. 686 (2016) 137–144.
[31] S. Cadot, O. Renault, M. Frégnaux, D. Rouchon, E. Nolot, K. Szeto, C. Thieuleux, L. Veyre, H. Okuno, F. Martin, E.A. Quadrelli, A novel 2-step ALD route to ultra-thin MoS_2 films on SiO_2 through a surface organometallic intermediate, Nanoscale 9 (2017) 538–546.
[32] B.D. Keller, A. Bertuch, J. Provine, G. Sundaram, N. Ferralis, J.C. Grossman, Process control of atomic layer deposition molybdenum oxide nucleation and sulfidation to large-area MoS_2 monolayers, Chem. Mater. 29 (2017) 2024–2032.
[33] Y. Zhan, Z. Liu, S. Najmaei, P.M. Ajayan, J. Lou, Large-area vapor-phase growth and characterization of MoS_2 atomic layers on a SiO_2 substrate, Small 8 (2012) 966–971.
[34] H.F. Liu, K.K.A. Antwi, J.F. Ying, S.J. Chua, D.Z. Chi, Towards large area and continuous MoS_2 atomic layers via vapor-phase growth: thermal vapor sulfurization, Nanotechnology 25 (2014) (405702-1-11).
[35] K.K. Liu, W. Zhang, Y.H. Lee, Y.C. Lin, M.T. Chang, C. Su, C.S. Chang, H. Li,

Y.M. Shi, H. Zhang, C.S. Lai, L.J. Li, Growth of large-area and highly crystalline MoS_2 thin layers on insulating substrates, Nano Lett. 12 (2012) 1538–1544.
[36] S. Najmaei, Z. Liu, W. Zhou, X.L. Zou, G. Shi, S.D. Lei, B.I. Yakobson, J.C. Idrobo, P.M. Ajayan, J. Lou, Vapour phase growth and grain boundary structure of molybdenum disulphide atomic layers, Nat. Mater. 12 (2013) 754–759.
[37] Y. Yu, C. Li, Y. Liu, L. Su, Y. Zhang, L. Cao, Controlled scalable synthesis of uniform, high-quality monolayer and few-layer MoS_2 films, Sci. Rep. 3 (2013) (1866-1-6).
[38] K.M. McCreary, A.T. Hanbicki, J.T. Robinson, E. Cobas, J.C. Culbertson, A.L. Friedman, G.G. Jernigan, B.T. Jonker, Large-area synthesis of continuous and uniform MoS_2 monolayer films on graphene, Adv. Funct. Mater. 24 (2014) 6449–6454.
[39] J. Jeon, S.K. Jang, S.M. Jeon, G. Yoo, Y.H. Jang, J.-H. Park, S. Lee, Layer-controlled CVD growth of large-area two-dimensional MoS_2 films, Nanoscale 7 (2015) 1688–1695.
[40] S. Cui, Z. Wen, X. Huang, J. Chang, J. Chen, Stabilizing MoS_2 nanosheets through SnO_2 nanocrystal decoration for high-performance gas sensing in air, Small 11 (2015) 2305–2313.
[41] S. Prezioso, F. Perrozzi, L. Giancaterini, C. Cantalini, E. Treossi, V. Palermo, M. Nardone, S. Santucci, L. Ottaviano, Graphene oxide as a practical solution to high sensitivity gas sensing, J. Phys. Chem. C 117 (2013) 10683–10690.
[42] F. Ricciardella, S. Vollebregt, T. Polichetti, M. Miscuglio, B. Alfano, M.L. Miglietta, E. Massera, G.D. Francia, P.M. Sarro, Effects of graphene defects on gas sensing properties towards NO_2 detection, Nanoscale 9 (2017) 6085–6093.
[43] N. Kumar, A.K. Srivastava, H.S. Patel, B.K. Gupta, G.D. Varma, Facile synthesis of ZnO–reduced graphene oxide nanocomposites for NO_2 gas sensing applications, Eur. J. Inorg. Chem. 2015 (2015) 1912–1923.